Accurate full-wave analysis of micromachined coplanar waveguides

Accurate Full-wave Analysis of Micromachined Coplanar Waveguides

P.G. van Leuven*, M.C. van Beurden and A.G. Tijhuis

Abstract — **We propose a full-wave mode-analysis method suited for micromachined coplanar waveguides (MCPWs). This method is based on the mixed-potential integral equation, in combination with a zero-search algorithm. Results are presented for a semicircular step-index fibre as well as for a MCPW.**

1 INTRODUCTION

As operating frequencies reach several GHz in modern IC-technology, transporting signals requires waveguiding structures, such as coplanar waveguides (CPWs), to allow for confinement of the fields. However, at these high frequencies, the Silicon used in CMOS-technology exhibits non-negligible losses and dispersion that limit the use of such waveguides. To overcome these limitations, the concept of micromachining, the process of selectively removing substrate material, has been investigated by several authors [1–3].

The coplanar waveguide (CPW) has several advantages over other types of waveguides as it can be manufactured with a single mask and allows for stacked-layer designs. It supports an 'even' and an 'odd' propagating quasi-TEM mode, of which the 'odd'-mode is generally undesired as it leaks energy. In a conventional CPW, losses occur at the edges of the center conductor where the field strength is highest. The micromachined CPW (MCPW) is essentially a conventional CPW where the substrate has been etched away in the gaps between the conductors, as shown in Fig. 1. This results in grooves with a shape depending on the applied etch method. Another key advantage is that the MCPW does not need additional support structures after micromachining.

In modeling such structures, a finite element method (FEM) would be a conceptually straightforward approach to analyze the effect of these grooves and their shape on the propagating modes. Hence, finding the propagating (and nonpropagating) modes is then equivalent to an eigenvalue analysis of a linear system. However, these waveguides typically have sub-wavelength dimensions, which would result in a rather large number of unknowns for a FEM compared to the domain of interest. Especially near the edges of the conductors mesh refinement is required to capture the singular field behavior. Therefore, a full-wave modeling approach has been developed based on boundary integral equations (BIEs) and equivalence principles. By using BIEs, the number of unknowns reduces significantly as the 2D-problem is effectively reduced to a 1D-problem, as only the boundary needs to be discretized. Further, radiation conditions are automatically included. An important drawback, however, is that the determination of the propagation coefficients for each mode involves a nonlinear search procedure. However, we will show that such a nonlinear search procedure can be carried out rather efficiently for homogeneous subdomains.

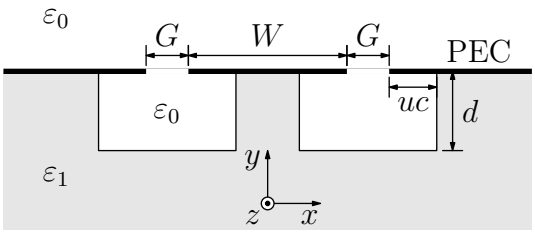

Figure 1: Schematic representation of a cross-section of a micromachined coplanar waveguide, with U-shaped grooves.

2 FORMULATION

For the formulation of the waveguide problem, we will assume a common factor $e^{j\omega t-\gamma_z z}$ for all field components, where ω is the angular frequency and γ_z is the complex wave number in the invariant z-direction. This common factor is assumed implicitly and is therefore omitted from all equations. Hence, we may replace $\nabla \rightarrow \nabla_t - \gamma_z \hat{\boldsymbol{z}}$ and $\partial_t \rightarrow j\omega$. Further, we will separate all longitudinal and transverse field components in Maxwell's equations, e.g. $\boldsymbol{E} = \boldsymbol{E}_t + E_z\hat{\boldsymbol{z}}$, to which we apply the correct boundary conditions. Each homogeneous subdomain is separated upon the introduction of equivalent electric and magnetic boundary sources, i.e. Love's equivalence principle. Hence, the electric field in each sub-domain can be written in mixed

*Eindhoven University of Technology, Den Dolech 2, Postbus 513, 5600MB Eindhoven.
e-mail: p.g.v.leuven@tue.nl, tel.: +31-(0)40-2473436.

978-1-4244-3386-5/09/$25.00 ©2009 IEEE

potential form as

$$\boldsymbol{E} = -j\omega\mu\boldsymbol{A} + (j\omega\varepsilon)^{-1}(\nabla_t - \gamma_z\hat{\boldsymbol{z}})\Phi - (\nabla_t - \gamma_z\hat{\boldsymbol{z}}) \times \boldsymbol{F}, \quad (1)$$

where $\boldsymbol{A}$ and $\boldsymbol{F}$ are the magnetic and electric vector potentials respectively, and Φ is the electric scalar potential. A similar equation holds for the magnetic field $\boldsymbol{H}$. Traditionally, we will write the potentials as

$$\{\boldsymbol{A}, \boldsymbol{F}\} = \int_{\mathcal{C}} \underline{\underline{\boldsymbol{G}}}(\boldsymbol{\rho}, \boldsymbol{\rho}') \cdot \{\boldsymbol{J}', \boldsymbol{M}'\} dl', \quad (2)$$

$$\Phi = \int_{\mathcal{C}} G^{\Phi}(\boldsymbol{\rho}, \boldsymbol{\rho}') \left[(\nabla_t' - \gamma_z\hat{\boldsymbol{z}}) \cdot \boldsymbol{J}'\right] dl', \quad (3)$$

where $\boldsymbol{\rho} = x\hat{\boldsymbol{x}} + y\hat{\boldsymbol{y}}$ and $\boldsymbol{\rho}' = x'\hat{\boldsymbol{x}} + y'\hat{\boldsymbol{y}}$ denote the observation and source coordinates respectively. Further, $\underline{\underline{\boldsymbol{G}}}$ represents the appropriate Green's function and, $\boldsymbol{J}' = \boldsymbol{J}(\boldsymbol{\rho}')$ and $\boldsymbol{M}' = \boldsymbol{M}(\boldsymbol{\rho}')$ denote the equivalent electric and magnetic boundary sources. Then, by adding the equations for the outer and inner regions in a PMCHW manner, a total system of equations is formed, leading to a mixed-potential integral equation MPIE.

2.1 Green's function for the electric mirror

Consider two half spaces separated by a perfectly conducting (PEC) sheet at $y = 0$. For such a configuration, the spatial Green's function can be written as a direct term and a reflected term. Therefore we introduce the spatial Green's function

$$\underline{\underline{\boldsymbol{G}}}^{\pm}(\boldsymbol{\rho}, \boldsymbol{\rho}') = \underline{\underline{\boldsymbol{I}}} G(\boldsymbol{\rho}, \boldsymbol{\rho}') \pm (\hat{\boldsymbol{x}}\hat{\boldsymbol{x}} - \hat{\boldsymbol{y}}\hat{\boldsymbol{y}} + \hat{\boldsymbol{z}}\hat{\boldsymbol{z}}) G(\boldsymbol{\rho}, \boldsymbol{\rho}'_m), \quad (4)$$

where $\underline{\underline{\boldsymbol{I}}}$ is the unit operator, $G(\boldsymbol{\rho}, \boldsymbol{\rho}') = (2\pi)^{-1} K_0(\gamma_t |\boldsymbol{\rho} - \boldsymbol{\rho}'|)$, with K_0 being the modified Bessel function of the second kind of order 0, $\gamma_t = \sqrt{-\omega^2\varepsilon\mu - \gamma_z^2}$ and $\boldsymbol{\rho}'_m = x'\hat{\boldsymbol{x}} - y'\hat{\boldsymbol{y}}$ i.e. the mirrored source point. The $\pm$ is needed for the different response to the electric sources $\boldsymbol{J}$ (-) and the magnetic sources $\boldsymbol{M}$ (+) in Eq.(2).

2.2 Mode searching

After applying a Galerkin type method-of-moments (MoM) on the MPIE, the moment-matrix Z is formed. This reduces the mode-searching problem to an eigenvalue problem, hence we are looking for non-trivial solutions to $Z(\gamma_z)\boldsymbol{x} = 0$. This will only occur at certain values of γ_z, corresponding to the modes pertaining to the configuration. As we will allow for lossy media, $\varepsilon = \varepsilon' - j\varepsilon''$ these (propagating) modes are complex. By choosing $f(\gamma_z) = \det(Z(\gamma_z))$ as a characteristic function in combination with the argument principle, we are able to determine the number of zeros within a certain contour in the complex domain. Hence, by choosing a rectangle in which we expect to find modes, it is possible to bisect the rectangle until a desired number of zeros is located within a certain (sub-)rectangle. Then, a Newton method is employed to search for the actual zero(s) within the (sub-)rectangle. After the zero has been found an eigenvalue analysis is performed that leads to the corresponding eigenvector.

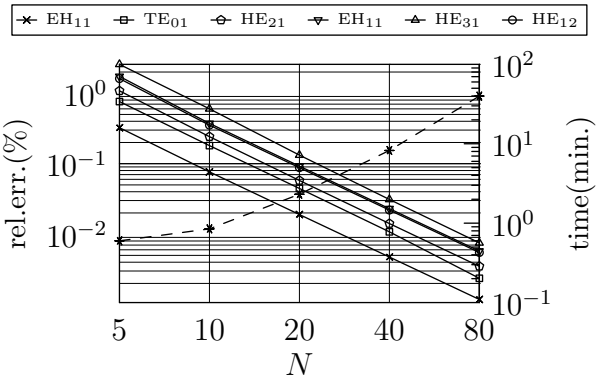

Figure 2: Convergence of the mode numbers for increasing number of segments for a stepindex fibre with core $\varepsilon_1 = 2\varepsilon_0$ and cladding ε_0 at normalized frequency $v = 4.7123$. Further the dashed line indicates the computation time.

3 RESULTS

3.1 Semicircular step-index fibre with PEC mirror

As a validation and benchmark test, consider a step-index fibre that has been cut in half and where a PEC sheet has been placed on the cutting edge. The modes pertaining to a conventional step-index fibre are known through an analytically available equation in [4, Section 8.9]. The effect of placing the PEC mirror is that the hybrid modes (HE and EH) that normally have a double multiplicity now have a single multiplicity. Further, TM-modes can no longer exist as the PEC mirror forces the radial electric field to vanish. The wavenumbers for the propagating modes will lie on the imaginary axis such that $\omega\sqrt{\varepsilon_0\mu_0} \leq \mathrm{Im}(\gamma_z) \leq \omega\sqrt{\varepsilon_1\mu_0}$. Consequently the search rectangle is chosen around the imaginary axis. In Fig. 2 the relative error in wavenumber compared to the exact values is given for increasing number of segments. Also, the computation time is shown. The computations were performed on a dual-core 3.0GHz Intel Xeon pro-

cessor with 4GB of RAM, without using parallelization.

3.2 MCPW

Finally, we will investigate the loss reduction after micromachining a CPW. We start from a conventional CPW with dimensions $W = 30\ \mu m$, $G = 8\ \mu m$, $d = 0\ \mu m$, and $uc = 0\ \mu m$ for which we will find the wavenumber (γ_z) of the 'even'-mode at 20 GHz. The Si-substrate has material parameters $\varepsilon_r = 11.4$ and a resistivity of 20 Ω-cm. Then we compare the attenuation constant, $\alpha_z = \mathrm{Re}(\gamma_z)$, of the CPW to two MCPWs with the same etch depth (d) with and without underetching (uc). The results are shown in Table 1. Although the attenuation constant is slightly higher ($\approx 10\%$) than the measured results published in [3, Fig.12], we do achieve similar loss reduction. The difference might be due to our model, since we assume ground planes of infinite extent in the transverse direction and do not account for finite substrate thickness, whereas the fabricated MCPW has finite dimensions. Further, the actual Si-substrate should be modelled with more accurate parameters.

$d(\mu m)$	$uc(\mu m)$	α_z(dB/mm)	loss red.
0	0	1.62	-
15	0	1.06	34.8%
15	14	0.41	74.8%

Table 1: Reduction of loss after micromachining a CPW, with different underetch.

4 CONCLUSIONS

We have developed a numerical model, which allows for accurate full-wave analysis of MCPW waveguides. Further, we have shown that the mode-search procedure can be carried out within acceptable time limits. Lastly, the loss reduction after micromachining a CPW has been demonstrated.

ACKNOWLEDGMENTS

The authors would like to thank Marion Matters and John Mills of the Electronics Systems & Silicon Integration (ESSI) group at *Philips Research* for their support.

References

[1] D. Williams and S. Schwarz, "Reduction of propagation losses in coplanar waveguide," vol. 84, no. 1, pp. 453–454, 1984.

[2] K. Herrick, T. Schwarz, and L. Katehi, "Si-micromachined coplanar waveguides for use in high-frequency circuits," *Microwave Theory and Techniques, IEEE Transactions on*, vol. 46, no. 6, pp. 762–768, Jun 1998.

[3] L. Leung, W.-C. Hon, J. Zhang, and K. Chen, "Characterization and attenuation mechanism of CMOS-compatible micromachined edge-suspended coplanar waveguides on low-resistivity silicon substrate," *Advanced Packaging, IEEE Transactions on*, vol. 29, no. 3, pp. 496–503, Aug. 2006.

[4] S. Ramo, J. R. Whinnery, and T. V. Van Duzer, *Fields and Waves in Communication Electronics.* Wiley, January 1994.